HHS Public Access

Author manuscript

Science. Author manuscript; available in PMC 2022 March 22.

Published in final edited form as:

Science. 2022 February 11; 375(6581): 639–647. doi:10.1126/science.abh0474.

An autonomously swimming biohybrid fish designed with human cardiac biophysics

Keel Yong Lee[1,†], **Sung-Jin Park**[1,2,†], **David G. Matthews**[3], **Sean L. Kim**[1], **Carlos Antonio Marquez**[1], **John F. Zimmerman**[1], **Herdeline Ann M. Ardoña**[1,‡,§], **Andre G. Kleber**[4], **George V. Lauder**[3], **Kevin Kit Parker**[1,5,6,*]

[1]Disease Biophysics Group, John A. Paulson School of Engineering and Applied Sciences, Harvard University, Boston, MA 02134, USA.

[2]Biohybrid Systems Group, Coulter Department of Biomedical Engineering, Georgia Institute of Technology and Emory University School of Medicine, Atlanta, GA 30322, USA.

[3]Museum of Comparative Zoology, Harvard University, Cambridge, MA 02138, USA.

[4]Beth Israel Deaconess Medical Center, Harvard Medical School, Boston, MA 02115, USA.

[5]Wyss Institute for Biologically Inspired Engineering, Harvard University, Boston, MA 02115, USA.

[6]Harvard Stem Cell Institute, Harvard University, Cambridge, MA 02138, USA.

Abstract

Biohybrid systems have been developed to better understand the design principles and coordination mechanisms of biological systems. We consider whether two functional regulatory features of the heart—mechanoelectrical signaling and automaticity—could be transferred to a synthetic analog of another fluid transport system: a swimming fish. By leveraging cardiac mechanoelectrical signaling, we recreated reciprocal contraction and relaxation in a muscular bilayer construct where each contraction occurs automatically as a response to the stretching of an antagonistic muscle pair. Further, to entrain this closed-loop actuation cycle, we engineered an electrically autonomous pacing node, which enhanced spontaneous contraction. The biohybrid fish

[*]**Corresponding author.** kkparker@seas.harvard.edu.
[†]These authors contributed equally to this work.
[‡]Present address: Department of Chemical and Biomolecular Engineering, Henry Samueli School of Engineering, University of California Irvine, CA 92697, USA.
[§]Present address: Sue and Bill Gross Stem Cell Research Center, University of California, Irvine CA 92697, USA.

Author contributions: K.Y.L. and S.-J.P. conceived and designed the study, developed a geometrically insulated cardiac tissue node-integrated muscular bilayer construct, designed and performed performance experiments, analyzed data, organized figures, and wrote the paper. K.K.P. conceived and designed the study, developed the idea of a geometrically insulated cardiac tissue node and muscular bilayer, and supervised the project. A.G.K. and G.V.L. contributed to the concept of a geometrically insulated cardiac tissue node and muscular bilayer, respectively. D.M. and G.V.L. contributed to the PIV experiments of both biohybrid and wild-type fish. S.L.K. designed optogenetic tools and edited the manuscript. C.M. assisted the fabrication of the biohybrid fish. S.L.K., J.Z., and H.A.M.A. performed primary neonatal rat ventricular harvest for the biohybrid fish optimization. All authors contributed to the preparation of the manuscript

Competing interests: K.Y.L., S.-J.P., A.G.K., V.T., and K.K.P. are inventors on a patent filed by Harvard University, U.S. Provisional Patent Application No. 63/299,920, based on the results described in this manuscript. The remaining authors declare no competing interests.

SUPPLEMENTARY MATERIALS
science.org/doi/10.1126/science.abh0474

equipped with intrinsic control strategies demonstrated self-sustained body–caudal fin swimming, highlighting the role of feedback mechanisms in muscular pumps such as the heart and muscles.

Circulatory systems in living organisms are intricately designed to transport blood throughout the body. Their most basic function is fluid transport, and a diversity of similar fluid pumping mechanisms and designs are found throughout nature (1). Fluid pumps in vertebrates, considered broadly, range from a human circulatory system with closed vessels within which fluid moves, to oscillatory fluid mechanisms in aquatic species in which fluid is transported along the body to generate propulsive thrust. Inspired by these distinct but similar natural processes, we and others have developed biohybrid analogs of an external fluid pump capable of mimicking the locomotion of aquatic species (2-4). The underlying motivation for developing biohybrid systems capable of reproducing biological behaviors is to better understand the design principles and coordination mechanisms of biological systems, although the performance of these systems has been lacking in comparison to natural fluid transport pumps (4).

A key feature of aquatic species is closed-loop actuation of antagonistic musculature that provides control over the direction of momentum transfer from the body muscles to the fluid, enabling efficient locomotion. Similarly, in the circulatory system, muscles of the heart dynamically respond to physiological demands through internal feedback systems and impart momentum to drive fluid motion. Mechano-electrical signaling and cardiac automaticity play an essential role in regulating the contractile pace and strength in a closed-loop control system (Fig. 1, A to C). Mechanoelectrical signaling (5, 6) is hypothesized to regulate intracardiac feedback, which allows cardio-myocytes (CMs) to adaptively respond to dynamic mechanical pressures (7, 8) by inducing changes in electrophysiology through stretch-activated mechanosensitive proteins (9, 10) (Fig. 1B). Automaticity of the heart stems from the sinoatrial node, which is structurally and functionally insulated from the surrounding myocardium (11-13) and initiates spontaneous electrical activity in the absence of an external stimulus and without direct neural intervention (Fig. 1C).

We reasoned that using principles of cardiac control systems to design a biohybrid platform could result in a fluid pumping system with comparable efficiencies to natural fishlike fluid pumping systems. Leveraging fundamental features of cardiac function allows for autonomous self-pacing and independent motion control while providing the basis for a closed-loop design that mimics aquatic swimming systems. We designed, built, and tested a biohybrid fish equipped with an antagonistic muscular bilayer and a geometrically insulated cardiac tissue node (G-node) with human stem cell–derived CMs or neonatal rat ventricular CMs (Fig. 1, D to F) to test the ability of a biohybrid system to control the movement of fluids with biological levels of performance. To integrate mechanoelectrical signaling of CMs in a simplified biohybrid platform, we recreated asynchronous muscle contractions (Fig. 1D) based on insect muscles (fig. S1) (14). In insects, each contraction results automatically from a response to the stretching of an antagonistic muscle pair, generating self-sustained muscle contraction cycles. In the muscular bilayer construct of the biohybrid fish (Fig. 1D), CMs are electrically connected within each side and mechanically coupled across sides, so that the shortening of contracting muscles on each side directly translates

to axial stretching of the opposite side muscle, leading to antagonistic muscle excitations and contractions. To replicate the electrically insulated structure of a sinoatrial node (Fig. 1C) (15), we functionally isolated a small number of CMs (the source) in the G-node (Fig. 1E) with a single exit pathway that allows for an electrical connection between the G-node and muscle tissues (the sink). This facilitated the activation of large downstream quiescent muscle cells (sink) with a small number of activating CMs (source) by reducing the impedance between source and sink (11-13, 15, 16). Together, the muscular bilayer and G-node in the biohybrid fish (Fig. 1F) enabled the generation of continuous rhythms to regulate its antagonistic muscle pair to produce spontaneous yet coordinated body–caudal fin (BCF) propulsion swimming.

Antagonistic contraction of muscular bilayer construct

We developed a muscular bilayer construct by modifying hydrogel-based muscular thin films (16-18). The double-sided micromolded gelatin thin film (200 μm thick) was engineered by sandwiching a gelatin and crosslinker (microbial transglutaminase) mixture between two polydimethylsiloxane stamps with line groove features (25 μm ridge width, 4 μm groove width, and 5 μm groove depth). CMs were then seeded onto both sides of the micromolded gelatin so that they could self-assemble as laminar, anisotropic muscle with engineered cellular alignment, characteristic of the ventricular myocardium (Fig. 1, G and H).

To demonstrate independent activation between the muscular bilayer tissues, we used lentiviral transduction to express blue-light–sensitive (ChR2) (19) and red-light–sensitive (ChrimsonR) (20) ion channels in each muscle layer (Fig. 1, H and I, fig. S2, and movie S1). Alternating blue-and-red light stimulation (15-ms pulses of 450 and 620 nm light, respectively) activated ChR2- and ChrimsonR-expressing muscle layers independently. The shortening of contracting muscles on each side was transduced to produce antagonistic bending stress and oscillate the muscle construct along the longitudinal axis (fig. S3 and movie S2). The contractions and relaxations of muscular bilayer muscles were decoupled at low pacing frequencies (e.g., 1 and 1.5 Hz), but at higher pacing frequencies (e.g., 2.5 and 3 Hz), the relaxation of one side started to overlap with the subsequent contraction of the other side (fig. S3 and movie S2). The overlapping, fast, active contraction of the opposite-side muscle considerably increased the oscillating speed of the muscular bilayer construct (fig. S3), preventing diastolic stress development that single-layered muscular thin films exhibit at high pacing frequencies (17, 18). These antagonistic muscle contractions in the muscular bilayer construct permitted large peak-to-peak amplitudes over a wide range of pacing frequencies (fig. S3), in contrast to single-layered muscular thin films (17, 18).

Integration of the muscular bilayer into biohybrid fish

The muscular bilayer construct was integrated into the biohybrid fish (16) by means of tissue engineering techniques (fig. S4). Inspired by fish musculoskeletal structure (fig. S5), we created an asymmetrical body along both the antero-posterior and dorso-ventral axes while maintaining sagittal symmetry through a fivelayered architecture. From left to right (Fig. 1J), the biohybrid fish consists of (i) a layer of aligned muscle tissue made of human stem

cell–derived CMs, (ii) a rigid paper layer in the anterior body and caudal fin fabricated by laser ablation, (iii) a compliant gelatin layer in the posterior body cast by means of a threedimensional elastomer polydimethylsiloxane mold, (iv) a second paper layer, and (v) a second aligned muscle tissue layer for forming the antagonistic muscle pair. The passive component of the biohybrid fish is made up of paper (thickness 190 μm; Young's modulus 4 GPa; density 1.2 g/ml), the gelatin body (thickness 192.22 ± 1.95 μm; Young's modulus 56 kPa; density 1.5 g/ml), and a plastic floater fin (thickness 1 mm; Young's modulus 1.3 GPa; density 0.833 g/ml) was designed to maintain directional body stability and neutral buoyancy while minimizing drag during forward swimming. The large surface area of the floater fin combined with the relatively heavy weight of the hydrogel insert in the anterior ventral portion of the body helped the fish maintain an upright orientation. Neutral buoyancy was achieved by adjusting the size of the plastic floater fin, thereby matching the average density of the biohybrid fish to the media in which it was suspended. The active component of the biohybrid fish consists of a muscular bilayer construct on the flexible posterior gelatin hydrogel body and operates as a single self-propelling system through coordinated contraction of muscle tissues. The final overall design (fig. S6) consists of 73,000 live CMs in a hydrogel-paper composite body 14 mm in length and 25.0 mg of total mass, including 0.36 mg muscle mass (fig. S7).

Optogenetically induced BCF propulsion

To characterize system-level kinematics of the muscular bilayer, we controlled antagonistic muscle contractions in the biohybrid fish by external optogenetic stimulation (Fig. 2). We stimulated the muscular bilayers by alternating blue and red light-emitting diode light pulses (Fig. 2A) while the bilayers were submerged in a 37°C Tyrode's salt solution containing glucose. As shown in the video-tracking analysis (Fig. 2, B to H, and movie S3), the biohybrid fish (i) initiated contraction of the muscle tissue on the left side upon red light stimulation and produced a peak oscillation amplitude in the tail (Fig. 2, B, F, and I); (ii) induced contraction of the muscle tissue on the right side after blue light stimulation (180° phase shift between red and blue lights); (iii) recovered its tail at a near-straight position (Fig. 2, C and G) and reached peak thrust production (Fig. 2I); (iv) oscillated its tail with peak amplitude right before a subsequent red light stimulation (Fig. 2, D and I); and (v) rebounded back to a near-straight position (Fig. 2E) generating maximal thrust (Fig. 2I). As shown by the lateral deflection (Fig. 2H), the body curvature (Fig. 2J), and swimming displacement (Fig. 2K), the biohybrid fish generated rhythmic forward thrust reproducing BCF propulsion. The biohybrid fish deformed its posterior body with a single bend while switching between positive and negative posterior body curvature upon light stimulation. The biohybrid fish oscillated its fin instead of generating a bending body wave because optical stimulation induced a simultaneous global muscle contraction. The relatively stiff anterior body and caudal fin resisted deformation from fluid forces. This allowed the biohybrid fish to exhibit asymmetric body deformation in which the largest lateral deflections and curvatures occurred in the posterior body between 0.5 and 0.8 of total length (Fig. 2J), in a manner reminiscent of BCF swimmers (fig. S8).

Antagonistic muscle contractions of the biohybrid fish generated a hydrodynamic signature similar to those of wild-type BCF swimmers—specifically, the water flow in the wake of

and around the fish bodies, which we visualized with particle image velocimetry (PIV) (Fig. 2, B to H, fig. S8). The biohybrid fish shed two vortex pairs per tail-beat cycle and one pair per lateral tail excursion (movie S3), one of the key characteristic flow patterns of BCF swimmers (movies S4 to S6). Each lateral tail excursion from bent to near-straight positions induced strong wake flows that formed a visible vortex pair with the opposite rotational direction (Fig. 2, B and C, vortices 1 and 2′; Fig. 2, D and E, vortices 2 and 3′; and Fig. 2, F and G, vortices 3 and 4). When the vortex pair reached the tail from the posterior body, it was shed (Fig. 2D, vortices 1 and 2′; Fig. 2F, vortices 2 and 3′) and continuously moved away from the fish body under its own momentum (Fig. 2, D to G, vortices 1 and 2′; and Fig. 2, F and G, vortices 2 and 3′).

The inclusion of a muscular bilayer architecture improved the high-frequency swimming of the biohybrid fish. Our optogenetically controlled biohybrid fish (6.4-mm-long muscle tissue body) responded up to 3 to 4 Hz (fig. S9 and movie S7), maintained a large tail-beat amplitude and angle, and exhibited a positive pacing frequency and tail beat angular-speed relationship (fig. S9). The biohybrid fish made of human stem cell–derived CMs (movie S7) and primary neonatal rat ventricular CMs (fig. S10 and movie S8) exhibited increased swimming speeds with increasing pacing frequencies (Fig. 2L) reminiscent of the force-frequency relationship of the heart. By contrast, a previous biohybrid stingray (3) exhibited reduced swimming speeds at high pacing frequencies as it had single-layered muscle and lacked antagonistic muscle contractions. The upper limit of optogenetic pacing frequency that induces a 1:1 stimulus response is also affected by body dimensions: a longer-bodied fish (8.2 mm; fig. S6C) exhibited oscillatory motion up to 2 Hz, but not at 2.5- and 3-Hz stimulation (movie S9).

Autonomous BCF propulsion

We tested whether reconstructing antagonistic muscle contractions with CMs could sustain spontaneous rhythmic contractions by means of mechanoelectrical signaling (Fig. 3A). Spontaneous activation and contraction on one side of the 49-day-old biohybrid fish led to a subsequent antagonistic contraction on the opposite side through mechanical coupling between muscle tissues (Fig. 3B and movies S10 and S11). These spontaneous antagonistic contractions led to alternating bending motions of the posterior body (Fig. 3, C to E), resulting in rhythmically sustained forward displacement (Fig. 3D) as shown in optogenetically triggered body–caudal fin propulsions (Fig. 2). Notably, biohybrid fish with a larger tail-beat angle had a higher probability to induce a subsequent muscle contraction (Fig. 3F), suggesting that the lengthening of one muscle layer caused by a shortening of the other muscle layer directly induced subsequent contractions through cardiac mechanoelectrical signaling. We treated the biohybrid fish with stretch-activated ion channel inhibitors [streptomycin (21) and gadolinium (Gd^{3+}) (22) (movies S12 and S13). We observed that these inhibitors disrupted antagonistic contractions in the biohybrid fish by breaking the positive relationship between peak tail-beat angle and probability of antagonistic contractions (Fig. 3F and fig. S11). Further, frequency-domain analysis showed that the spontaneous frequencies of streptomycin- and Gd^{3+}-treated muscular bilayer tissues were not harmonic (fig. S12). Stretched-activated ion channel inhibition

decreased swimming speeds (Fig. 3G), which demonstrated that mechanoelectrical signaling mediates self-sustainable spontaneous rhythmic contractions in muscular bilayers.

We tested whether reconstructing a geometrically distinct and electrically insulated node could initiate spontaneous electrical activity as a result of the automaticity of CMs in the absence of an external stimulus. Inspired by the partial electrical insulation of a sinoatrial node (15), we created the G-node (Fig. 1E), where a small number of CMs are structurally and functionally isolated with a single exit pathway. The G-node is electrically coupled by gap junctions (12, 23) to muscle tissues and facilitates progressive activation of large quiescent neighboring muscle cells (sink) by a small number of activating CMs (source). The geometrical design of both the G-node and the sink is crucial in determining the leading muscle activation site, because the electrical current being exchanged between individual CMs of different membrane potentials can be reflected at the tissue edges (12, 16). Thus, we hypothesized that the reflection of intracellular currents at the perimeter of the G-node would synchronize the spontaneous activity and initiate coordinated pacemaking from the G-node.

To decouple the effect of antagonistic muscle contractions from muscle activation at the G-node, we mechanically restricted muscle movement with laboratory tape on a glass slide and determined muscle activation through calcium imaging (24). CMs in the G-node and four corners [anterior ventral corner (AV), anterior dorsal corner (AD), posterior ventral corner (PV), and posterior dorsal corner (PD) (figs. S13 and S14)] of the muscle tissue overcame source-sink mismatch and initiated muscle activation (Fig. 3, H and I, figs. S13 and S14, and movies S14 and S15). As we hypothesized, the G-node predominantly activated the muscle construct over the other four corners of the muscle tissue (Fig. 3, I and J, and figs. S13 and S14). Comparing two G-node sizes showed that a larger G-node containing ~1700 cells increased the probability of initial muscular activation at the G-node compared with the smaller G-node with a pointed node (~600 cells) (fig. S13 and movie S15), suggesting that a group of geometrically distinct CMs are needed to initiate muscular activation. Additionally, rounding the sink's corners decreased the probability of activation at the corners (fig. S14A) by increasing the number of downstream cells at each respective corner (fig. S15), but the G-node's corner design did not affect the probability of activation at the G-node (fig. S14B), which indicates that acute angles in small source tissue such as the G-node are not critical in determining the activation site. Rather, this suggests that a larger perimeter-to-area ratio of the G-node synchronized electrical interaction between the geometrically distinct CMs through reflections of electrotonic currents and produced a relatively fast and synchronized activation over the sink tissue. Acute angled anterior corners of the fish body increased the probability of activation at the anterior side (Fig. 3J) by decreasing the number of downstream cells (fig. S15), thus allowing cells on the anterior side (G-node and anterior corners AD and AV) to predominantly initiate spontaneous activation waves (60% from the G-node and 97% from all anterior sides; Fig. 3J).

However, upon removing the restrictions on muscle movement, the G-node primarily acted as a secondary mechanism for controlling contractions. Only when the antagonistic muscle contractions were minimal would the G-node initiate sequential local muscle activation and contraction, leading to undulatory locomotion (fig. S16A and movie S17).

However, in subsequent muscle contractions the biohybrid fish predominantly exhibited simultaneous global contractions and oscillatory locomotion with minimal body wave propagations, caused by mechanoelectrical signaling of the muscular bilayer (Fig. 3E, fig. S16, B and C, and movie S16). Although G-nodes are located on both sides of the body, one dominant G-node controlled initiation of muscle contraction as a secondary pacemaker (movie S17). Because of the G-node's role as a secondary pacing mechanism of antagonistic contractions, the biohybrid fish equipped with a G-node had significantly increased spontaneous contractile frequencies (Fig. 3K) while maintaining similar body kinematics (fig. S16) and a positive frequency–swimming speed relationship similar to those of externally stimulated fish (Fig. 3L). As a result, our G-node-equipped biohybrid fish demonstrated increased maximum swimming speeds of more than one body length per second (15 mm/s; movie S11).

Although these G-node–entrained, mechano-electrical signaling–sustained, cyclic antagonistic muscle contractions are autonomous, optogenetic stimulation can be used for on-demand locomotion control. Antagonistic muscle contractions became coupled with optical pacing within fewer than three sequential light pulses (movie S18). Further, optogenetic stimulation can also be used to inhibit autonomous locomotion; pausing immediately after a pulsed stimulation can stop muscle contractions for an extended period (50 s; movie S19). Prolonged continuous optogenetic stimulation stops muscle contractions and autonomous locomotion (movie S20). External stimulation reinitiates autonomous, antagonistic muscle contractions by activating mechanoelectrical signaling (movie S21).

Advanced performance of the biohybrid fish

Our autonomously swimming biohybrid fish (15.0 mm/s; movie S11) outperformed the locomotory speed of previous biohybrid muscular systems (2, 3, 25-35) [5 to 27 times the speed of the biohybrid stingray (3) and the biohybrid skeletal muscle biorobot] (32) (Fig. 4A), highlighting the role of feedback mechanisms in developing biohybrid systems. Moreover, when considering the ratio of muscle mass to the total weight for the biohybrid fish (1.4%; fig. S7) and biohybrid stingray (9.7%) (3), the biohybrid fish demonstrated faster swimming speeds per unit muscle mass by an order of magnitude (13 times the maximum swimming speed of the biohybrid stingray) (3) (Fig. 4B).

The swimming performance of the biohybrid fish resembles that of wild-type BCF swimmers with similar body lengths (juvenile zebrafish, juvenile white molly, and *Microdevario kubotai*) (Fig. 4, C to F, fig. S8, and movies S4 to S6). Similar to the biohybrid fish, each of these species moves by shedding a pair of reverse-sign vortices when their tails reach maximum lateral excursion (Fig. 4, C to F). The strength of these vortices between the biohybrid and wild-type fish were comparable (Fig. 4, C to F). Rather than forming a continuous chaotic chain of wakes, both the biohybrid and wild-type fish maintain stable vortex pairs with minimal vortex interactions (Fig. 4, C to F). The stable wake pattern is a typical characteristic of juvenile zebrafish locomotion at relatively high Strouhal numbers (St) and relatively low Reynolds numbers ($Re < 5000$) (36), where viscous forces cannot be neglected and the lateral velocity of wake flows are relatively high. In this flow regime, the swimming speed is nearly proportional to the tail-beat frequency (37).

Thus, the juvenile zebrafish, white molly, and *M. kubotai* had faster tail-beat frequencies (16.7, 7.5, and 7.7 Hz, which were 4.6, 2.1, and 2.1 times as high as that of the biohybrid fish) and showed proportionally increased swimming speeds of 59.7, 25.1, and 21.3 mm/s, respectively (4.0, 1.7, and 1.5 times as high as that of the biohybrid fish). Although muscle function in wild-type fish encompasses more than locomotion, when considering the ratio of total muscle mass to the total weight of biohybrid fish (1.4%; fig. S7) compared with wild-type fish (80%) (38), the maximum swimming speed per unit muscle mass of biohybrid fish exceeded those of wild-type fish by a factor of 70 to150 (Fig. 4B).

Efficiency of the biohybrid fish

To analyze the efficiency of the biohybrid fish, we used scaling and dimensional analysis. Wild-type swimmers achieved energetically favorable locomotion through convergent evolution and were found to hew to the two scaling relationships $St \sim Re^{-1/4}$ and $Re \sim Sw^{-1/4}$ in the low Re and high St flow regime (37) (Fig. 4, G and H). The Strouhal number $St = fA/U$ (f, tail-beat frequency; A, tail-beat amplitude; U, forward speed) represents the ratio of the lateral oscillation amplitude to swimming distance per lateral tail excursion, the swimming number $Sw = 2\pi fAL/\nu$ (L, characteristic body length of the swimmer; ν, fluid viscosity) represents input kinematics, and the Reynolds number $Re = UL/\nu$ compares inertial to viscous forces and is a function of swimming speed. Compared with the biohybrid stingray (3), our biohybrid fish operates much closer to these average scaling relationships of wild-type swimmers. Moreover, the biohybrid fish swimming at high tail-beat frequencies (high St and Sw) performed comparably to wild-type swimmers (Fig. 4, G and H).

The performance of the biohybrid fish is very sensitive to muscle kinematics and coordination. Some biohybrid fish accelerated by increasing tail-beat amplitude (figs. S17 and S18A and movie S22), which is similar to the acceleration of wild-type fish (39). This positive relationship between swimming speed and tail-beat amplitude during accelerative locomotion contrasts with the constant tail-beat amplitude regardless of swimming speed during steady locomotion (fig. S9B). Although St, Sw, and Re numbers increase with its swimming speed (fig. S18, B and C) in the accelerative locomotion, the biohybrid fish exhibited a considerable decrease in propulsive efficiency as its speed increases as shown by the deviation from the optimal St-Re and Re-Sw relationships of aquatic swimmers (fig. S18, B and C). The inhibition of muscle coordination with a stretch-activated ion channel blocker, Gd^{3+}, also led to a drastic reduction of 80.8% in Re and 40.6% in Sw and the deviation from optimal St-Re and Re-Sw relationships of aquatic swimmers (figs. S12 and S18, D to F, and movie S12), which demonstrate that muscular coordination is necessary to achieve effective and efficient swimming.

Long-term performance of the biohybrid fish

Given the autonomous antagonistic muscle contractions of the biohybrid fish, we questioned whether this spontaneous activity would improve its long-term performance. The biohybrid fish maintained spontaneous activity for 108 days [16 to 18 times the length of the biohybrid stingray (6 days) (3) and the skeletal muscle-based biohybrid actuator (7 days) (40)], equivalent to 38 million beats (Fig. 5, A and B, and movies S23 and S24). Further,

its locomotion could also be controlled by external optogenetic stimulation (movie S24) throughout this time. The autonomously swimming biohybrid fish also increased muscle contraction amplitude, maximum swimming speed, and muscle coordination for the first month before maintaining its swimming performance over 108 days (Fig. 5C). By contrast, biohybrid fish equipped with single-layered muscle showed deteriorating tail-beat amplitude within the first month (Fig. 5C and movie S25). These data demonstrate the potential of muscular bilayer systems and mechanoelectrical signaling as a means to promote maturation of in vitro muscle tissues.

Discussion

We integrated two functional design features of the heart—mechanoelectrical signaling and automaticity—into a biohybrid platform and recreated an autonomously actuating cardiac muscular system in the form of a biohybrid fish. This fish is a closed-loop system in which muscle contraction–induced bending is used as a feedback input to the endogenous mechanosensors—stretch-activated ion channels—in the muscles. These channels respond to this feedback input and induce muscle activation and contraction, producing self-sustainable rhythmic BCF propulsion. The self-driven spontaneous contractions in our muscular bilayer induced coordinated global tissue-level contractions with comparable efficiencies to wild-type fish. Alternatively, integrated optogenetic control enabled overriding of internal control mechanisms to stop and control asynchronous muscle contractions. There are few, if any, closed-loop mechanical fish robots that are free-swimming; fish robots also typically require numerous actuators and sensors to control fin movements, and these are difficult to engineer at smaller size scales (millimeters to centimeters scale) (41). However, integration of the cardiac activation system as an embedded mechanism of both sensing and control enabled the generation of fishlike locomotion at such smaller scales (42). The use of biological muscle actuators with intrinsic closed-loop control simplifies the construction compared with current mechanical robotic systems and provides control beyond existing biohybrid systems.

Additionally, our muscular bilayer construct provides a platform for studying tissue-level cardiac biophysics. We demonstrate that dynamic axial stretching can induce excitations and contractions on a beat-by-beat basis in engineered human stem cell–derived CM tissues by contributing to antagonistic muscle contractions. We found that antagonistic contractions are sensitive to streptomycin and Gd^{3+}, which indicates that mechanoelectrical signaling by means of stretch-activated ion channels is one of the essential mechanisms that mediate antagonistic contractions. Notably, in normal myocardium where CMs are mechanically and electrically coupled, mechanoelectrical signaling contributes to synchronizing local ventricular repolarization and protects against cell-to-cell repolarizations and contractile heterogeneities across the heart (43). By contrast, in our muscular bilayer where antagonistic muscle pairs are mechanically coupled yet electrically decoupled across sides, mechanoelectrical signaling generates stretch-induced depolarizations on a beat-by-beat basis. The stretch-induced excitations and contractions were also observed in quiescent single CMs and in a resting ventricular myocardium (10), but these observations were restricted to the ectopic responses of CMs to acute mechanical stimulation, which induced re-entrant arrhythmias. Our muscular bilayer construct is the first to demonstrate that

the mechanoelectrical signaling of CMs could induce self-sustaining muscle excitations and contractions for extended periods (108 days, equivalent to 38 million beats). These findings are aligned with the growing appreciation for cardiac stretch-activated channels and mechanoelectrical signaling mechanisms as targets of heart rhythm management (10, 44). The longevity of the autonomously moving fish system also raises the question of whether a feedback between repetitive electrical and mechanical activity and the regulation of its molecular elements through altered gene expression or other basic cellular processes is correlated.

The G-node, an isolated cluster of cells connected through a single conducting exit pathway, initiated spontaneous activation waves by reducing the impedance between source and sink. G-node integration improved locomotion speeds by enhancing the pacing frequency. This increased frequency in the presence of the G-node is reminiscent of entrainment in re-entry cycles in which the focus shortens the re-entry cycle (45). Another possible underlying mechanism of the increased frequency is that the G-node produced regular contractions and consequently induced stronger and more rapid contractions of the muscular bilayer, which could enhance the dynamics of antagonistic, asynchronous muscle contractions. The G-node functionality as a node of automaticity in the biohybrid fish suggests that, functionally, a pacemaker may be defined by its geometry and source-sink relationships as well as its ion channel expression.

Taken together, the technology described here may represent foundational work toward the goal of creating autonomous systems capable of homeostatic regulation and adaptive behavioral control. Our results suggest an opportunity to revisit long-standing assumptions of how the heart works in biomimetic systems, which may allow a more granular analysis of structure-function relationships in cardiovascular physiology.

Supplementary Material

Refer to Web version on PubMed Central for supplementary material.

ACKNOWLEDGMENTS

We thank M. Rosnach for photography and illustrations.

Funding:

this work was funded by the Harvard Paulson School of Engineering and Applied Sciences, the Wyss Institute for Biologically Inspired Engineering, National Institutes of Health National Center for Advancing Translational Sciences grant UH3TR000522, and National Science Foundation Materials Research Science and Engineering Center grant DMR-1420570. K.K.P. was sponsored by National Institutes of Health National Center for Advancing Translational Sciences grant 1-UG3-HL-141798-01. S.-J.P. was funded by the Georgia Institute of Technology and Emory University School of Medicine. G.V.L. was funded by the Office of Naval Research (T. McKenna, Program Manager, ONR 341), grant N00014-15-1-2234, and the National Science Foundation, grant 1830881. H.A.M.A. would like to thank the American Chemical Society for their generous support through the Irving S. Sigal Postdoctoral Fellowship. The views and conclusions contained in this document are those of the authors and should not be interpreted as representing the official policies, either expressed or implied, of the National Institutes of Health, the National Science Foundation, or the US Government. This work was performed in part at the Harvard Center for Nanoscale Systems, a member of the National Nanotechnology Infrastructure Network, which is supported by the National Science Foundation under award ECS-0335765. The Center for Nanoscale Systems is part of Harvard University.

Data and materials availability:

All data are available in the main text or the supplementary materials. Code and scripts are available at Zenodo (24)

REFERENCES AND NOTES

1. Vogel S, Vital Circuits: On Pumps, Pipes, and the Workings of Circulatory Systems (Oxford Univ. Press, 1992).
2. Nawroth JC et al., Nat. Biotechnol 30, 792–797 (2012). [PubMed: 22820316]
3. Park SJ et al., Science 353, 158–162 (2016). [PubMed: 27387948]
4. Ricotti L et al., Sci. Robot 2, eaaq0495 (2017). [PubMed: 33157905]
5. ter Keurs HE, Pflugers Arch. 462, 165–175 (2011). [PubMed: 21373861]
6. Quinn TA, Kohl P, Physiol. Rev 101, 37–92 (2021). [PubMed: 32380895]
7. Quinn TA, Kohl P, Ravens U, Prog. Biophys. Mol. Biol 115, 71–75 (2014). [PubMed: 24978820]
8. Dabiri BE, Lee H, Parker KK, Prog. Biophys. Mol. Biol 110, 196–203 (2012). [PubMed: 22819851]
9. Friedrich O, Wagner S, Battle AR, Schürmann S, Martinac B, Prog. Biophys. Mol. Biol 110, 226–238 (2012). [PubMed: 22959495]
10. Quinn TA, Jin H, Lee P, Kohl P, Circ. Arrhythm. Electrophysiol 10, e004777 (2017). [PubMed: 28794084]
11. Unudurthi SD, Wolf RM, Hund TJ, Front. Physiol 5, 446 (2014). [PubMed: 25505419]
12. Kléber AG, Rudy Y, Physiol. Rev 84, 431–488 (2004). [PubMed: 15044680]
13. Rohr S, Kucera JP, Fast VG, Kléber AG, Science 275, 841–844 (1997). [PubMed: 9012353]
14. Bullard B, Pastore A, Muscle Res J. Cell Motil. 32, 303–313 (2011).
15. Joyner RW, van Capelle FJ, Biophys. J 50, 1157–1164 (1986). [PubMed: 3801575]
16. Materials and methods are available as supplementary materials.
17. Park SJ et al., Circulation 140, 390–404 (2019). [PubMed: 31311300]
18. McCain ML, Agarwal A, Nesmith HW, Nesmith AP, Parker KK, Biomaterials 35, 5462–5471 (2014). [PubMed: 24731714]
19. Boyden ES, Zhang F, Bamberg E, Nagel G, Deisseroth K, Nat. Neurosci 8, 1263–1268 (2005). [PubMed: 16116447]
20. Klapoetke NC et al., Nat. Methods 11, 338–346 (2014). [PubMed: 24509633]
21. Gannier F, White E, Lacampagne A, Garnier D, Le Guennec JY, Cardiovasc. Res 28, 1193–1198 (1994). [PubMed: 7954622]
22. Yang XC, Sachs F, Science 243, 1068–1071 (1989). [PubMed: 2466333]
23. Kléber AG, Jin Q, Biophys. Rev 2, 031301 (2021). [PubMed: 34296210]
24. Lee KY et al. , Optical stimulation for independent activation of muscles: Matlab and Labview, Zenodo (2021); doi:10.5281/zenodo.5618323.
25. Feinberg AW et al., Science 317, 1366–1370 (2007). [PubMed: 17823347]
26. Xi J, Schmidt JJ, Montemagno CD, Nat. Mater 4, 180–184 (2005). [PubMed: 15654345]
27. Cvetkovic C et al., Proc. Natl. Acad. Sci. U.S.A 111, 10125–10130 (2014). [PubMed: 24982152]
28. Chan V et al., Sci. Rep 2, 857 (2012). [PubMed: 23155480]
29. Kim J et al., Lab Chip 7, 1504–1508 (2007). [PubMed: 17960278]
30. Akiyama Y, Hoshino T, Iwabuchi K, Morishima K, PLOS ONE 7, e38274 (2012). [PubMed: 22808004]
31. Akiyama Y et al., Biomed. Microdevices 14, 979–986 (2012). [PubMed: 22945325]
32. Pagan-Diaz GJ et al., Adv. Funct. Mater 28, 1801145 (2018).
33. Raman R et al., Proc. Natl. Acad. Sci. U.S.A 113, 3497–3502 (2016). [PubMed: 26976577]
34. Williams BJ, Anand SV, Rajagopalan J, Saif MT, Nat. Commun 5, 3081 (2014). [PubMed: 24435099]

35. Aydin O et al., Proc. Natl. Acad. Sci. U.S.A 116, 19841–19847 (2019). [PubMed: 31527266]
36. Taylor GK, Nudds RL, Thomas AL, Nature 425, 707–711 (2003). [PubMed: 14562101]
37. Gazzola M, Argentina M, Mahadevan L, Nat. Phys 10, 758–761 (2014).
38. Jackson HE, Ingham PW, Mech. Dev 130, 447–457 (2013). [PubMed: 23811405]
39. Wise TN, Schwalbe MAB, Tytell ED, J. Exp. Biol 221, jeb.190892 (2018).
40. Morimoto Y, Onoe H, Takeuchi S, Sci. Robot 3, eaat4440 (2018). [PubMed: 33141706]
41. Du R, Li Z, Youcef-Toumi K, Valdivia y Alvarado P, in Robot Fish: Bio-inspired Fishlike Underwater Robots, Du R, Li Z, Youcef-Toumi K, Valdivia P Alvarado y, Eds. (Springer, 2015), pp. 1–24.
42. Lauder GV, Tangorra JL, in Robot Fish: Bio-inspired Fishlike Underwater Robots, Du R, Li Z, Youcef-Toumi K, Valdivia P Alvarado y, Eds. (Springer, 2015), pp. 25–49.
43. Opthof T, Meijborg VM, Belterman CN, Coronel R, Cardiovasc. Res 108, 181–187 (2015). [PubMed: 25935868]
44. Quinn TA, Cardiovasc. Res 108, 1–3 (2015). [PubMed: 26209252]
45. Almendral J, Caulier-Cisterna R, Rojo-Álvarez JL, Pacing Clin. Electrophysiol 36, 508–532 (2013). [PubMed: 23305213]

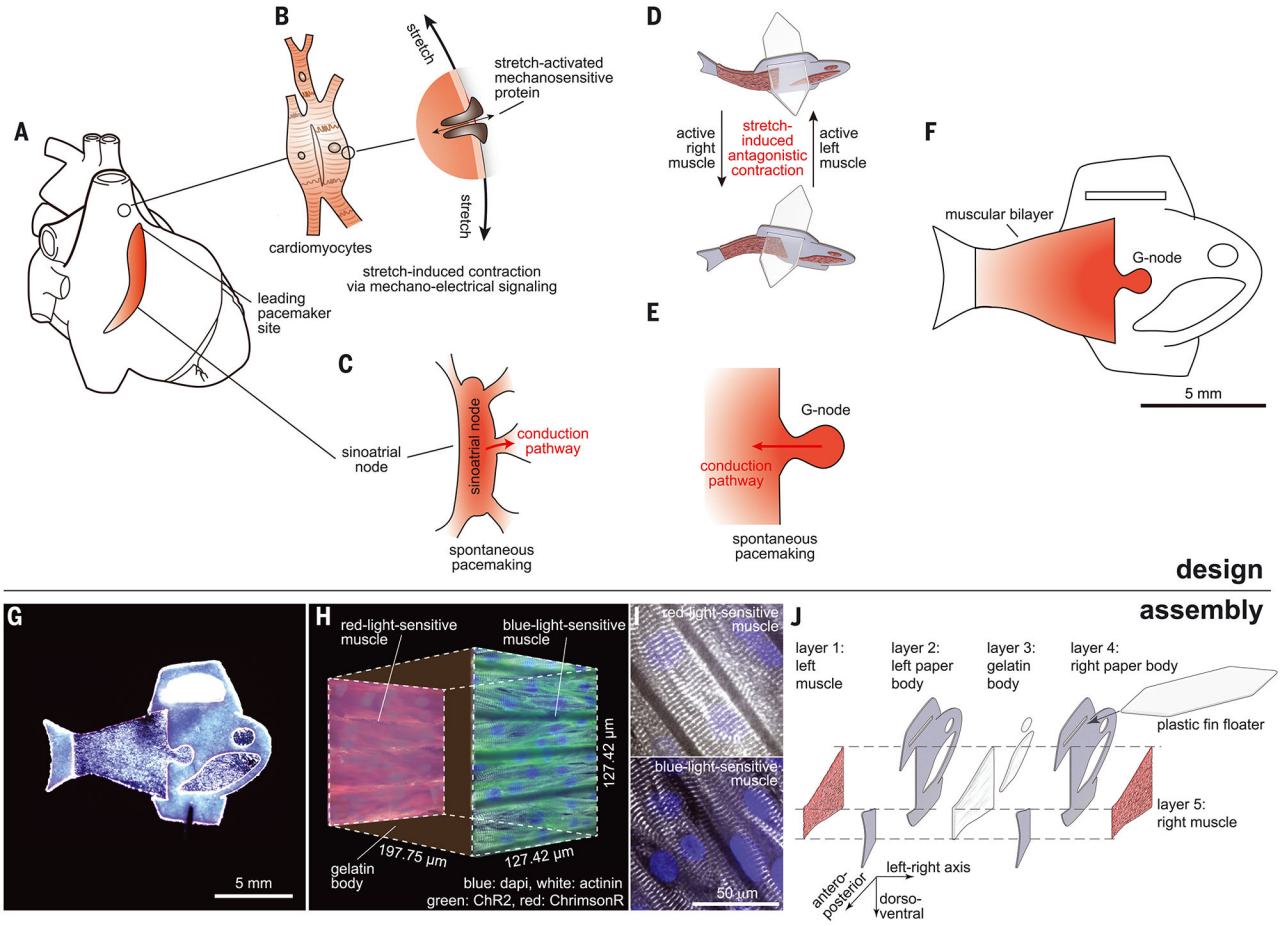

Fig. 1. Design and assembly of the biohybrid fish.

(**A**) Intrinsic autonomous muscle control of the heart. (**B**) Mechano-electrical signaling that adaptively responds to dynamic mechanical pressures by inducing changes in electrophysiology through stretch-activated mechanosensitive proteins. (**C**) Automaticity of the cardiac sinoatrial node, which is structurally and functionally insulated from the surrounding myocardium and initiates spontaneous electrical activity. (**D** to **F**) Autonomously swimming biohybrid fish. (D) Muscular bilayer in which the shortening of contracting muscles on each side directly translates to axial stretching of the opposite side muscle, leading to stretch-induced antagonistic muscle contractions. (E) G-node, where functionally isolated cardio-myocytes (CMs) generate spontaneous muscle activation rhythms. (F) Biohybrid fish equipped with the muscular bilayer and the G-node. (**G**) Image of the biohybrid fish made of human stem cell–derived CMs. (**H** and **I**) Muscular bilayer construct showing representative (H) mesoarchitecture and (I) microarchitecture. The gelatin posterior body was sandwiched by two muscle tissues expressing either a blue-light–sensitive opsin [ChR2 (green)] or a red-light–sensitive opsin [ChrimsonR (red)]. Representative immunostaining images of both tissues (sarcomeric alpha actinin, gray; nuclei, blue) show that Z-lines of the sarcomeres (the cell force-generating units) are perpendicular to the antero-posterior axis. (**J**) Five layers of body architecture: the body was symmetrical along the left-right axis but asymmetrical along both the antero-posterior

and dorso-ventral axis; this design was chosen to maintain directional body stability against roll and propel the body forward.

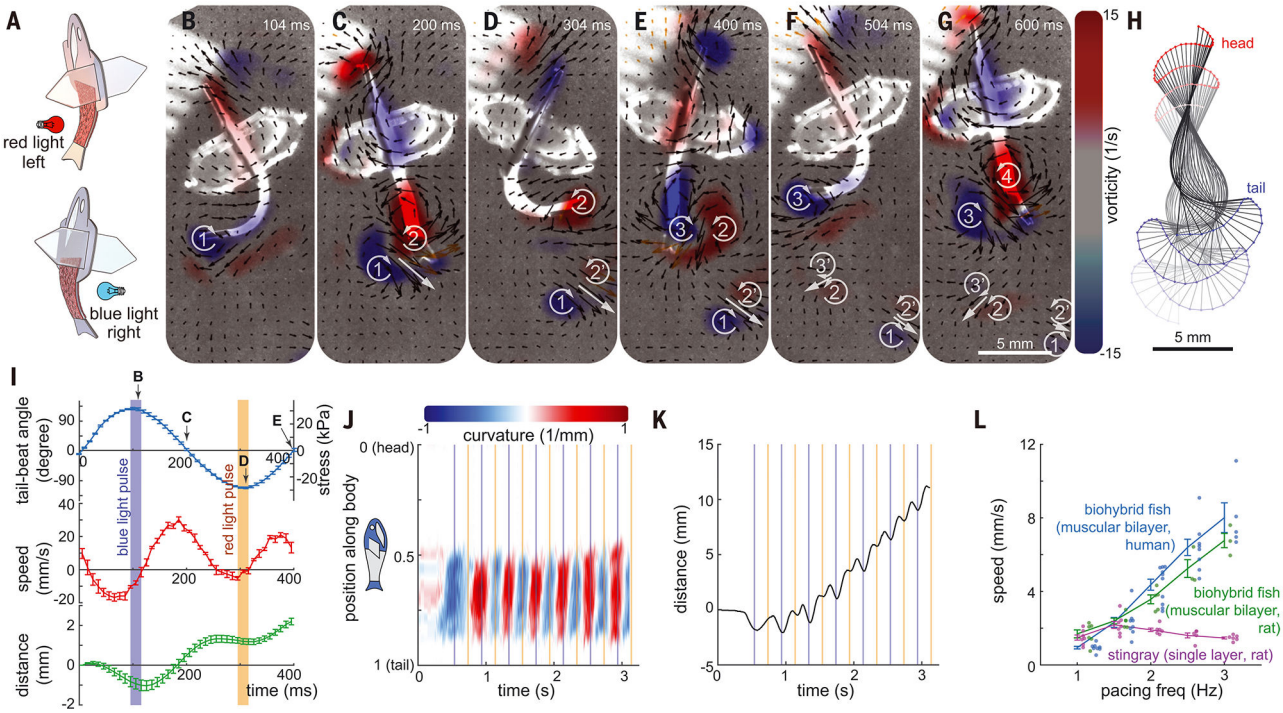

Fig. 2. Optogenetically induced BCF propulsion.

(**A**) Upon alternating blue and red light stimulation, the biohybrid fish induces contraction of the ChR2- and ChrimsonR-expressing muscles, respectively. (**B** to **G**) Body kinematics and hydrodynamics of the biohybrid fish during one and a half tail-beat cycles. (B and F) Peak contraction of left muscles. (C and G) recovery to straight position. (D) peak contraction of right muscle. (E) recovery to straight position. Left and right muscles work antagonistically against each other, leading to rhythmically sustained body and caudal fin (BCF) propulsion. PIV flow measurements highlight the shedding of the positive and negative vortex pair at every lateral tail excursion. (**H**) Corresponding midline kinematics (time step: 50 ms). (**I** to **K**) Kinematic analysis of seven strokes; correlation between optogenetic muscle activation and BCF locomotion (n = 7 strokes; data represent mean ± SEM). (J) aCurvature of the midline; (K) moving distance. (**L**) Positive relationship between pacing frequency and moving speed of optogenetically stimulated biohybrid fish [n = 31 videos from seven stingrays (3); 27 videos from six rat fish; and 54 videos from 12 human fish.] Data represent mean ± SEM).

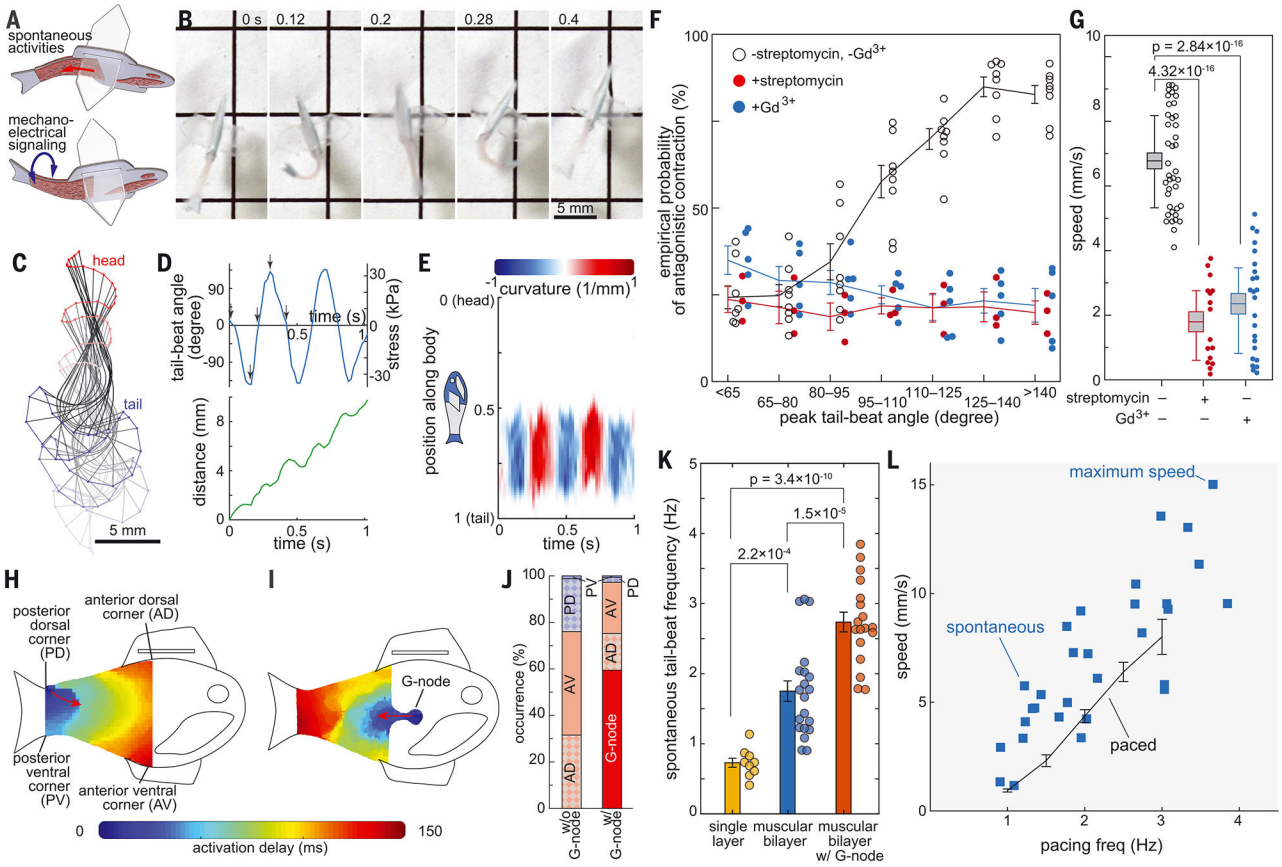

Fig. 3. Autonomous BCF propulsion.

(**A** to **G**) Mechano-electrical signaling of the muscular bilayer. (A) Spontaneous activation of one-side muscle induces consecutive contraction of the opposite-side muscle through mechano-electrical signaling between muscular bilayer tissues. (B) Representative time lapse images of consecutive antagonistic muscle contraction of 49-day-old biohybrid fish. (C) Midline kinematics (time step: 100 ms). (D) Correlation between spontaneous muscle activation and the moving distance. (E) Curvature of the midline during five consecutive left and right muscle strokes. (F) Empirical probability of antagonistic contraction and (G) moving speed of self-paced biohybrid fish treated with stretch-activated channel blockers, 250 μM streptomycin (n = 4 biohybrid fish) and 100 μM Gd^{3+} (n = 5 biohybrid fish) (box plot: center line, box limits, and whiskers indicates mean, SEM, and the first and third quartiles, respectively). The treatment of stretch-activated channel blockers, streptomycin and Gd^{3+} reduced the chance of antagonistic muscle contraction as well as the swimming speed of the biohybrid fish. (**H** to **L**) Geometrically insulated node (G-node). Activation pattern of biohybrid fish (H) without G-node and (I) with G-node. (J) Probability of muscle activation sites. Spontaneous muscle activation from G-node dominates spontaneous activation from the corners (n = 6 biologically independent samples without G-node and 5 samples with G-node). (K) Tail-beat frequency of biohybrid fish equipped with single-layer (n = 9 videos from nine fish), muscular bilayer (n = 20 videos from 14 fish), and muscular bilayer with G-node (n = 18 videos from five fish). Significance was determined by the Tukey-Kramer honestly significant difference test. (L) Positive relationship between pacing

frequency and moving speed of autonomously swimming biohybrid fish (n = 30 videos from 19 autonomously swimming biohybrid fish and 54 videos from optogenetically swimming biohybrid fish). Data represent mean ± SEM.

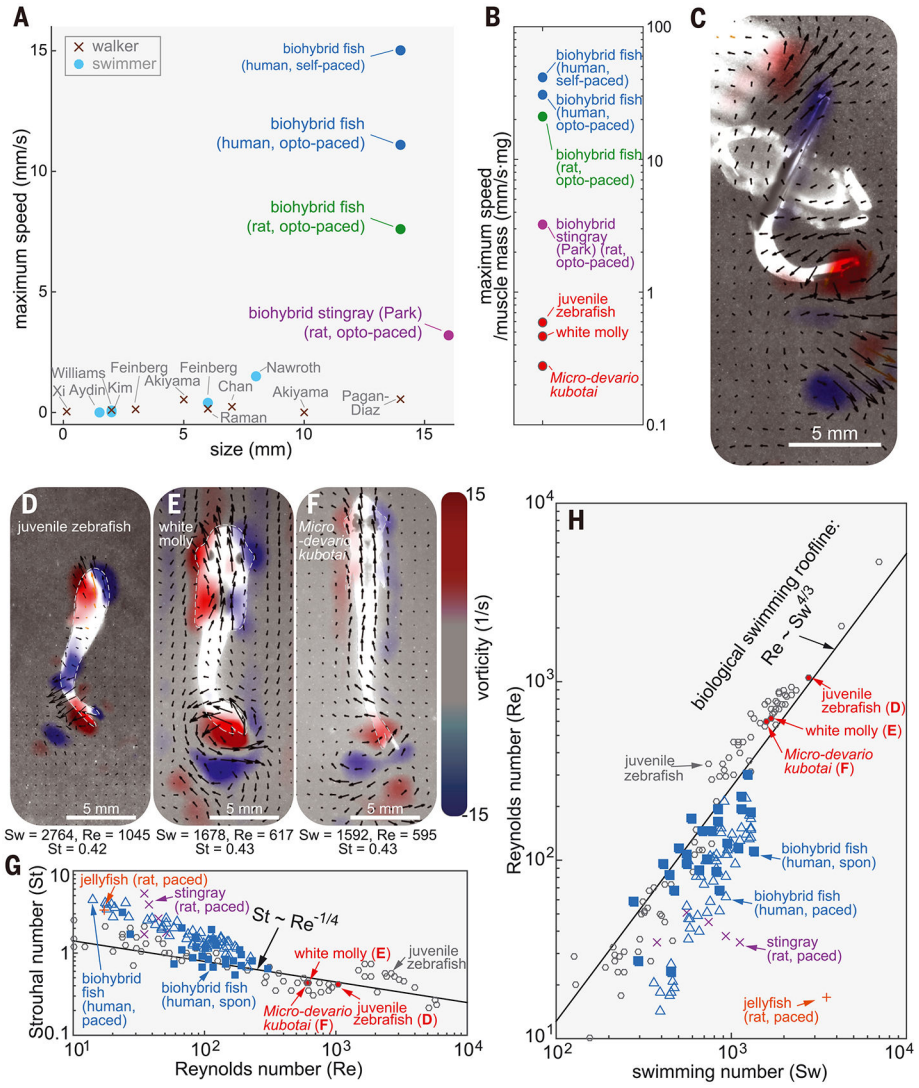

Fig. 4. Comparison of swimming performance between biohybrid and aquatic swimmers.

(**A** and **B**) Comparison of swimming performance in biohybrid walkers and swimmers. (A) locomotion speed (2, 3, 25-35) and (B) speed per unit muscle mass. PIV analysis of (**C**) biohybrid fish [body length (l_b): 14 mm]; (**D**) wild-type juvenile zebrafish (l_b: 12 mm); (**E**) white molly (l_b: 19 mm); and (**F**) and *M. kubotai* (l_b: 20 mm). (**G** and **H**) Scaling analysis of biohybrid fish and wild-type swimmers with (G) Re-St and (H) Sw-Re (n = 30 movies from 19 biohybrid fish).

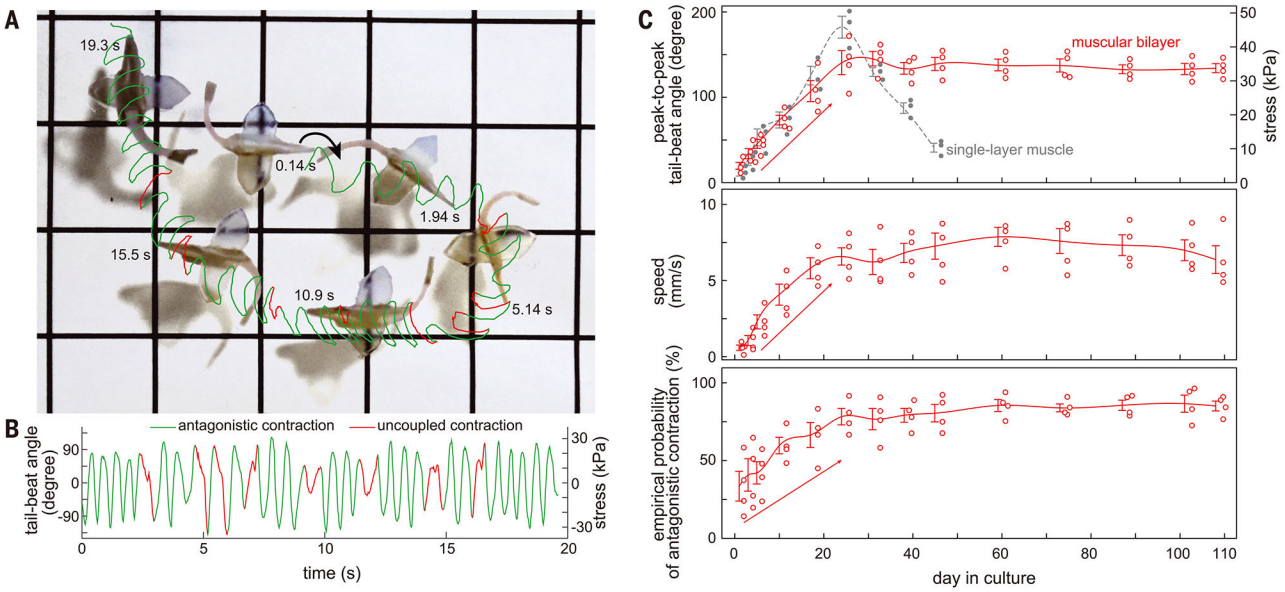

Fig. 5. Long-term swimming performance analysis.

(**A**) Trajectory (grids, 1 cm) and (**B**) corresponding tail-beat angle of 108-day-old biohybrid fish with 79% antagonistic contractions. (**C**) Swimming performance for 108 days ($n = 4$ fish). Biohybrid fish equipped with the muscular bilayer exhibited enhanced contracting amplitude, maximum swimming speed, and muscle coordination for the first month and maintained their performance for at least 108 days, whereas fish made with the single-layer muscle exhibited decreased contracting amplitude after 28 days. ($n = 4$ fish; data represent mean ± SEM).